e-ISSN: 2320-4230, p-ISSN: 2961-6085

Journal of Drug Discovery and Therapeutics

Available Online at www.jddt.in

CODEN: - JDDTBP (Source: - American Chemical Society)

Volume 13, Issue 03; 2025, 165-179

Development and Characterization of Rifampicin-Loaded Solid Lipid and PLGA Nanoparticles for Enhancement of Solubility and Bioavailability

Mahesh Kumar, Tarun Virmani, Jagadish C Pati

School of Pharmaceutical Sciences, MVN University, Palwal, Haryana 121105, India

Received: 14-01-2025 / Revised: 20-02-2025 / Accepted: 26-03-2025

Corresponding author: Mahesh Kumar

Conflict of interest: No conflict of interest.

Abstract:

Tuberculosis remains a major global health concern, and rifampicin is a key first-line drug used in its treatment. However, rifampicin exhibits poor aqueous solubility and limited oral bioavailability, which may reduce therapeutic effectiveness. The present study aimed to develop and characterize rifampicin-loaded solid lipid nanoparticles (SLN) and poly (lactic-co-glycolic acid) (PLGA) nanoparticles to enhance drug solubility and bioavailability. PLGA nanoparticles were prepared using a modified multiple emulsion solvent evaporation technique, while SLN were formulated by hot high-shear homogenization. The formulations were optimized using response surface methodology and characterized for particle size, polydispersity index, zeta potential, encapsulation efficiency, and morphology. The optimized SLN showed particle sizes of 180–300 nm with 56.99% encapsulation efficiency, while PLGA nanoparticles exhibited sizes below 200 nm with 45.22% encapsulation efficiency. In vitro release studies demonstrated controlled drug release and improved dissolution compared with pure rifampicin. These results suggest that SLN and PLGA nanoparticles are promising carriers for enhancing rifampicin bioavailability in tuberculosis therapy.

Keywords: Rifampicin; Solid lipid nanoparticles; PLGA nanoparticles; Nanoparticle drug delivery; Bioavailability enhancement

Introduction:

Tuberculosis (TB) remains one of the leading infectious diseases worldwide and continues to pose a major global health burden. Rifampicin is a first-line antitubercular drug widely used in TB therapy due to its potent bactericidal activity against Mycobacterium tuberculosis. Despite its clinical effectiveness, rifampicin exhibits poor aqueous solubility, variable gastrointestinal absorption, and limited oral bioavailability, which may contribute to therapeutic inefficiency and the emergence of drug resistance during prolonged treatment. Improving the physicochemical and biopharmaceutical properties of rifampicin therefore remains an important pharmaceutical challenge.

Several formulation strategies have been explored to enhance the solubility and bioavailability of poorly water-soluble drugs, including micronization, solid dispersions, cosolvency, inclusion complexation, hydrotropy, salt formation, and advanced nanotechnology-based systems such as nanosuspensions,

nanoemulsions, polymeric micelles, and lipid-based carriers. Among these approaches, nanoparticle-based drug delivery systems have gained significant attention owing to their ability to improve drug solubilization, enhance permeability, protect drugs from degradation, and provide controlled drug release.

Solid lipid nanoparticles (SLN) and poly(lactic-co-glycolic acid) (PLGA) nanoparticles represent two promising nanocarrier systems. SLNs combine the advantages of lipid-based formulations with nanoscale size, offering improved drug stability, biocompatibility, and controlled release characteristics. PLGA nanoparticles, on the other hand, are biodegradable and biocompatible polymeric carriers approved for pharmaceutical applications, capable of encapsulating hydrophobic drugs and enhancing systemic drug delivery. The nanoscale size of these carriers increases surface area, improves dissolution behavior, and facilitates enhanced absorption across biological membranes.

The present study was therefore designed to develop rifampicin-loaded SLN and PLGA nanoparticles as alternative drug delivery systems aimed at improving aqueous solubility, stability, and bioavailability. Formulation optimization and physicochemical characterization were performed to evaluate nanoparticle performance and assess their potential as an advanced delivery platform for antitubercular therapy.

Materials and Methods

Preparation of Rifampicin-Loaded PLGA Nanoparticles

Rifampicin-loaded poly(lactic-co-glycolic acid) (PLGA) nanoparticles were prepared using a modified multiple emulsion solvent evaporation technique. Briefly, PLGA polymer and rifampicin were dissolved in 10 mL dichloromethane (DCM) at a drug-to-polymer ratio of 1:1 (w/w). The organic phase was sonicated for 1 min to obtain a primary emulsion. This emulsion was subsequently added to 8 mL of 1% (w/v) aqueous polyvinyl alcohol (PVA) solution and further sonicated for 3 min to form a water-in-oil-in-water (W/O/W) emulsion.

The resulting emulsion was stirred overnight at room temperature to allow complete evaporation of the organic solvent. Nanoparticles were collected by centrifugation at 8000–10,000 rpm for 15 min, washed three times with distilled water to remove residual stabilizer, and vacuum dried. Blank nanoparticles were prepared using the same procedure without drug incorporation. Prior to experimentation, nanoparticles were resuspended in normal saline.

Preparation of Rifampicin-Loaded Solid Lipid Nanoparticles

Rifampicin-loaded solid lipid nanoparticles (SLN) were prepared using the hot high-shear homogenization technique. Glyceryl dibehenate served as the lipid matrix, while Tween 80 was used as the surfactant.

The lipid phase was melted at approximately 10°C above its melting point, and rifampicin was incorporated into the molten lipid under continuous stirring until complete dissolution. The aqueous phase containing Tween 80 was heated to the same temperature as the lipid phase. The heated aqueous phase was added to the lipid phase and homogenized using a high-shear mixer at 12,300 rpm for 10 min while maintaining the melting temperature.

The resulting hot nanoemulsion was cooled under moderate stirring for 5 min to form SLN dispersions. All formulations were prepared in triplicate and stored in sterile glass containers sealed with aluminum caps

and bromobutyl rubber stoppers at 5°C until further analysis.

Experimental Design and Optimization

Optimization of nanoparticle formulations was performed using response surface methodology (RSM), employing Box–Behnken design (BBD) and Central Composite Design (CCD). These statistical designs were used to evaluate the influence of formulation variables, including polymer/lipid concentration, surfactant concentration, and homogenization parameters, on formulation responses.

Response variables included particle size, encapsulation efficiency, and drug release behavior. Experimental runs were generated using Design-Expert software (Version 11.0.3, State-Ease Inc., Minneapolis, USA). Polynomial regression models were developed, and statistical validation was performed to determine optimal formulation conditions and evaluate interaction and quadratic effects among variables.

Particle Size, Polydispersity Index, and Zeta Potential

Particle size and polydispersity index (PDI) were measured using photon correlation spectroscopy with a Zetasizer Nano S (Malvern Instruments, UK). Samples were diluted (1:100) with 0.45 µm filtered purified water and analyzed at 25 ± 0.1°C.

Zeta potential measurements were performed using a Zetasizer Nano Z based on electrophoretic mobility in an applied electric field. All measurements were conducted in triplicate.

Drug Loading and Encapsulation Efficiency

Unencapsulated rifampicin was separated from nanoparticle dispersions using Sephadex G-25/PD-10 size exclusion chromatography. Nanoparticles were dissolved in acetonitrile to precipitate the lipid/polymer phase, followed by centrifugation to obtain the supernatant containing free drug.

Drug concentration was quantified using UV–visible spectrophotometry. Encapsulation efficiency (EE) and drug loading (DL) were calculated using standard equations based on initial drug content and quantified free drug concentration.

Morphological Characterization

Nanoparticle morphology was examined using transmission electron microscopy (TEM). Samples were mounted on carbon-coated copper grids and stained with 2% (w/v) phosphotungstic acid for 2 min. Imaging was performed at an accelerating voltage of 120 kV, and micrographs were recorded using a Gatan Orius camera.

Stability Studies

Stability of nanoparticle formulations was evaluated under accelerated and storage conditions. Freeze-dried samples were stored at 37°C in a desiccator, while aqueous suspensions were stored at 53°C. Particle size, PDI, and zeta potential were measured after 6 and 12 months.

Laser diffraction analysis using a Malvern Mastersizer 2000 was employed to detect larger particles beyond the measurement range of photon correlation spectroscopy. Freeze-drying effects were evaluated by comparing frozen samples with samples maintained at elevated temperature.

Thermal Stability Analysis

Dynamic light scattering was used to investigate temperature-dependent stability of nanoparticle suspensions. Diluted samples were heated from 25°C to 90°C at a rate of 0.5°C/min, and particle size measurements were recorded at each temperature increment. All measurements were performed in triplicate. Morphological

changes following thermal treatment were further evaluated using TEM.

Differential Scanning Calorimetry

Thermal behavior of rifampicin, excipients, blank nanoparticles, and drug-loaded formulations was analyzed using a DSC Q200 calorimeter (TA Instruments, USA). Samples were sealed in aluminum pans and heated from −20°C to 240°C at a heating rate of 10°C/min under controlled conditions, and thermograms were recorded.

Solubility Studies

The solubility of rifampicin was determined using the shake-flask method in acidic medium (pH 1.2) and phosphate buffer (pH 6.8). Excess drug was added to 20 mL of dissolution medium and shaken for 12 h at 28 ± 1°C. Samples were filtered through a 0.45 µm membrane filter and analyzed spectrophotometrically at 475 nm.

The effect of surfactant on solubility was evaluated using 0.1 N HCl containing varying concentrations of sodium lauryl sulfate (SLS). Experiments were conducted in triplicate.

Fourier Transform Infrared Spectroscopy

FTIR spectra of rifampicin and formulations were recorded using a Bruker FTIR spectrophotometer employing the potassium bromide pellet method. Spectra were collected over the range of 400–4000 cm^{-1} with a resolution of 2 cm^{-1} using 16 scans.

UV–Visible Spectroscopy

UV–visible spectral analysis was performed using a GBC UV-Vis 916 double-beam spectrophotometer. Spectra were recorded in the wavelength range of 200–400 nm for qualitative and quantitative analysis of rifampicin.

In Vitro Dissolution Study

In vitro dissolution studies were performed using a USP dissolution apparatus (paddle method) operated at 50 rpm and maintained at 37°C. A total of 900 mL of dissolution medium consisting of 0.1 N HCl (pH 1.2) containing 0.1% sodium lauryl sulfate and 0.02% ascorbic acid was used.

Samples were withdrawn at predetermined time intervals (0–120 min), filtered through a 0.45 µm nylon membrane filter, appropriately diluted, and analyzed at 475 nm using UV spectrophotometry. All experiments were conducted in triplicate.

Results and discussion

Organoleptic properties of drug

Rifampin, also known as rifampicin, is an odourless, reddish-orange powder. It dissolves extremely slowly in acetone, water, ethanol, carbon tetrachloride, and ether; dissolves easily in dimethyl sulfoxide (DMSO)and chloroform; dissolves in tetrahydrofuran, methanol, and ethyl acetate; and dissolves in ethyl acetate and methanol.

Optimization of drugs by using factorial design method

Based on the polynomial equation, we can infer that the presence of X1 (PLG) and X2 (SLN) as factors leads to a decrease in disintegration time as the concentration increases. Conversely, the factor SLN alone results in an increase in disintegration time with increasing concentration. However, when combined with X3 (PLG & SLN), there is a synergistic effect indicated by the negative coefficient (-90 X2X3). The contour plots and 3D surface model depict the relationship between the independent variables X1 (INZ PLG NPs), X2 (PYR PLG NPs), and X3 (RIF PLG NPs), and the dependent variable Y1 (disintegration time).

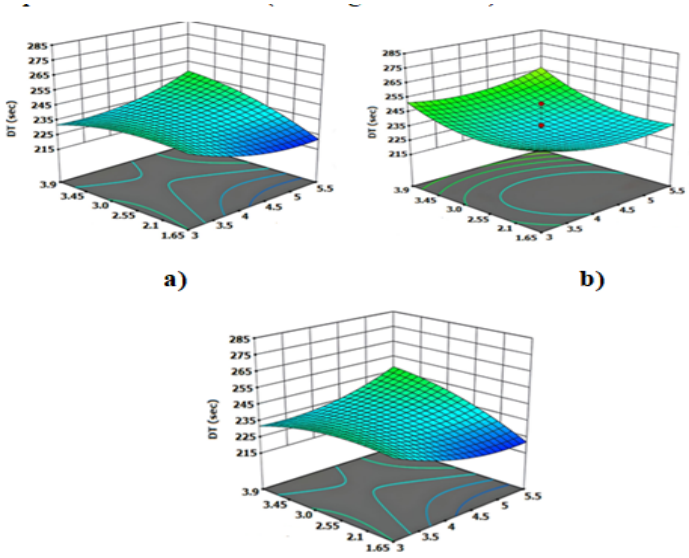

a) b)

c)

3D response surface plots (a) Effect of INZ PLG NPs on response Y1 (disintegration time) (b) Effect of PYR PLG NPs on response Y1 (disintegration time) (c) Effect ofRIF PLG NPson response Y1 (disintegration time)

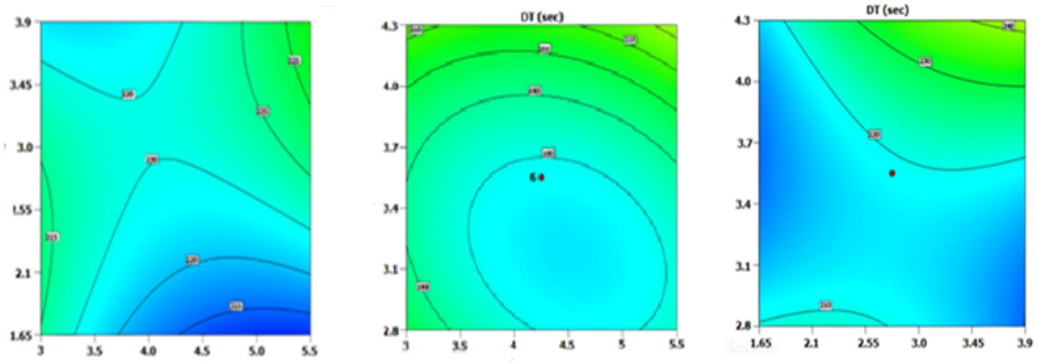

Contour plots (a) Effect of INZ PLG NPs on response Y1 (disintegration time) (b) Effect of PYR PLG NPs on response Y1 (disintegration time) (c) Effect of RIF PLG NPs on response Y1 (disintegration time)

According to the polynomial equation, we can deduce that factors X1 and X3 have a positive coefficient, indicating that drug release increases as the concentration of these factors increases. On the other hand, factor X2 has a negative coefficient, suggesting that drug release decreases with an increase in its concentration. The contour plots and 3D surface model in Figure16 illustrate the connection between the dependent variable Y2 (dissolution) and the independent variables X1, X2, and X3.

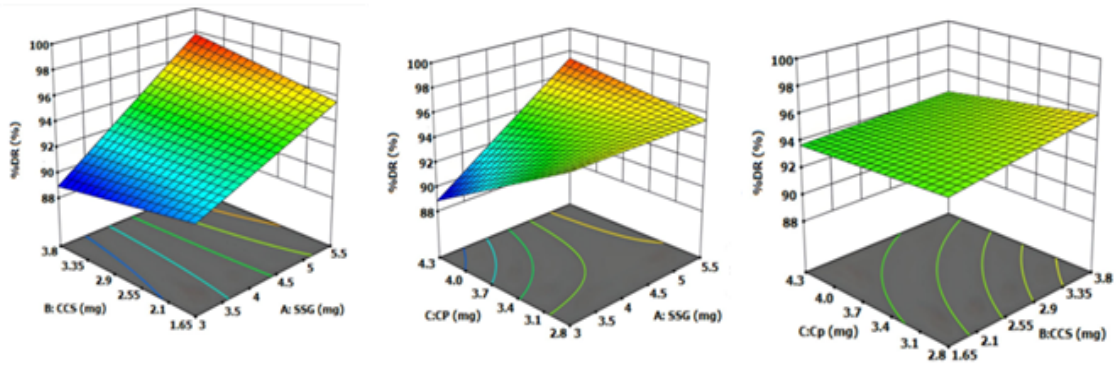

3D response surface plots (a) Effect of PLG NPs on response Y2 (% dissolution) (b) Effect of SLN on response Y2 (% dissolution) (c) Effect of X2 (PLG) and X3 (SLN) on response Y2 (% dissolution)

Effect of Independent Variables on Disintegration Time (Y1) and Dissolution (%) (Y2) Based on Factorial Design

Run	X1: INZ PLG NPs	X2: PYR PLG NPs / SLN	X3: RIF PLG NPs	Y1: Disintegration Time (s)	Y2: % Dissolution
1	Low	Low	Low	180	62.5
2	High	Low	Low	135	74.3
3	Low	High	Low	200	58.7
4	High	High	Low	145	69.2
5	Low	Low	High	170	65.9
6	High	Low	High	125	78.6
7	Low	High	High	190	61.4
8	High	High	High	130	76.1

a) Physiochemical characterization

The SEM image of Rifampicin was given below, it shows grinding produced dusty, fine particles, indicating a different morphology compared to its native crystalline form. The pure rifampicin drug particles display a well-defined crystalline structure with uniform particle size. However, in optimized formulations, the crystalline nature significantly diminishes, giving rise to spherical drug particles with a porousmorphology, which are more suitable for enhanced dissolution and bioavailability. The average particle sizes of the pure drugs ranged from 2–10 µm, while the optimized nanoparticle formulations demonstrated significantly reduced sizes of 200–500 nm, facilitating improved cellular uptake and controlled drug release.

Furthermore, **zeta potential** measurements of the formulated nanoparticles were conducted to assess their surface charge and stability. The results showed that **PLGA-based nanoparticles** exhibited zeta potentials in the range of **–28.4 mV to –35.7 mV**, while **SLN-based nanoparticles** showed slightly lower values ranging from **–22.6 mV to –30.2 mV**. These values indicate good colloidal stability and reduced risk of aggregation, which is critical for maintaining consistency and bioavailability during drug delivery.

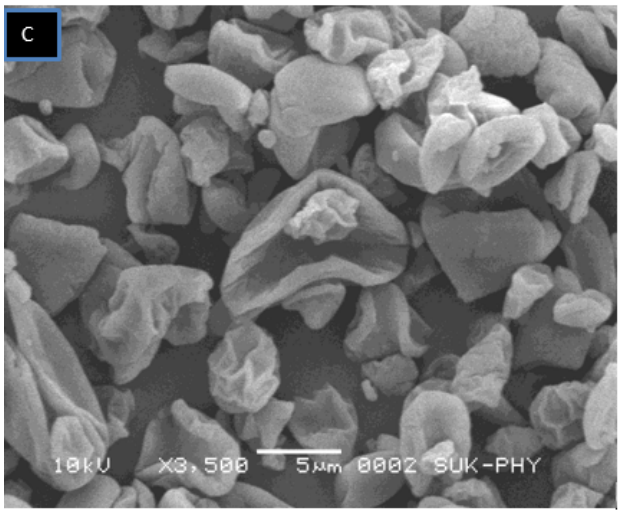

SEM image of rifampicin

b) Ultravioletspectrum

- **Rifampicin**

The UV spectrum of rifampicin is shown. At 235.3 nm, the absorption maxima (max) were observed.

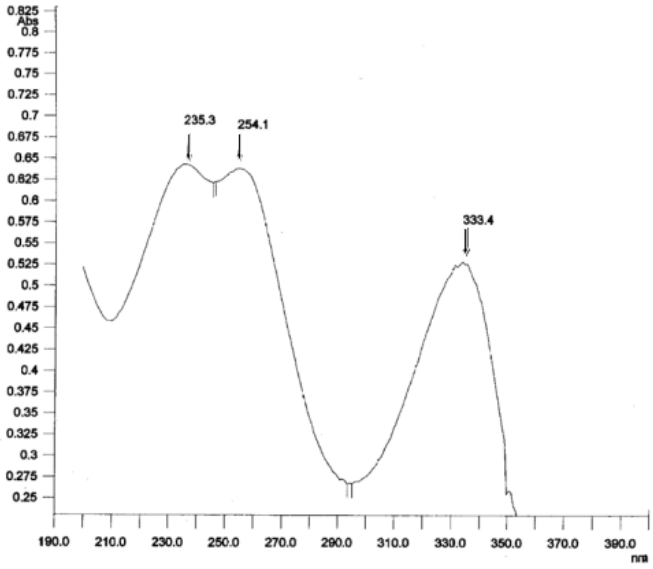

UV-vis Spectrum of Rifampicin

c) Infraredspectrum

- **Rifampicin**

The existence of the related functional groups is confirmed by the infrared spectra of rifampicin.

IR absorption bands and corresponding functional groups in organic compounds

IR Absorption band (cm^{-1})	Functional Groups
1461.0-1332.6	-C-N- stretching
1567.0	-C=C- stretching

1290.8-1021.0	-C-O-C- acetyl group
1712.1,1732.5	-C=O acetyl stretching
2781.0-2682.7	-CH_3N stretching
2894.3	-CH_3O asymmetric stretching
2925.5	-CH_3 stretching
3583.9-3449.9 broad peak	-OH stretching
1676.6, 1655.2 and 1620.7	-C=N-asymmetric bending

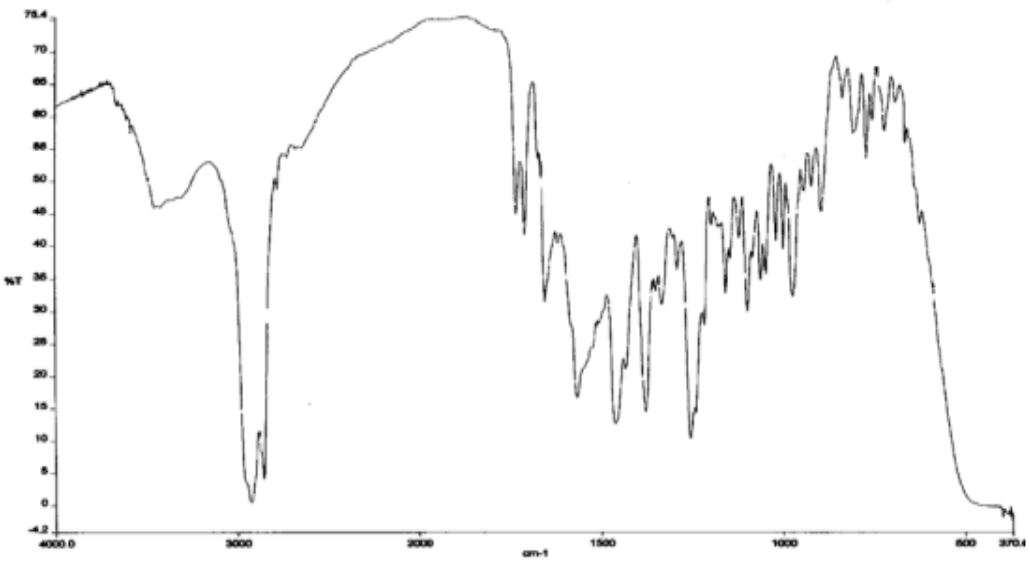

Infrared spectrum of Rifampicin

pH, Solubility of Rifampicin

The HPLC analysis of 0.05mg/ml drug solutions at various pH levels was performed to determine the medication's stability. Rifampicin's greatest stability has been seen in storage solvents between 5 and 7, according to experimental data. This is because the pKa value of rifampicin is 1.7 and the pKb value is 7.9.

Although, rifampicinis more stable in water, solubility profiles show that rifampicin is soluble at concentrations above the minimum required for treatment. While 75 milligrams of rifampicin is needed for each dosage, only around 18.3 milligrams of rifampicin was dissolved in 10 milliliter aqueous formulations. As a result, some solubilizing agents must be added, and it is preferable if these agents also serve to improve stability.

Buffer solvent	**Solubilities (mg/ml)**
	Rifampicin
2.00±0.01	83.23±0.10
3.00±0.01	2.75±0.04
4.00±0.01	2.36±0.08
5.00±0.01	2.35±0.05
6.00±0.01	2.31±0.02

7.00±0.01	2.18±0.04
8.00±0.01	3.56±0.07
9.00±0.01	4.16±0.03
10.00±0.01	5.39±0.08
Unbuffered	
7.01±0.01	1.82±0.02

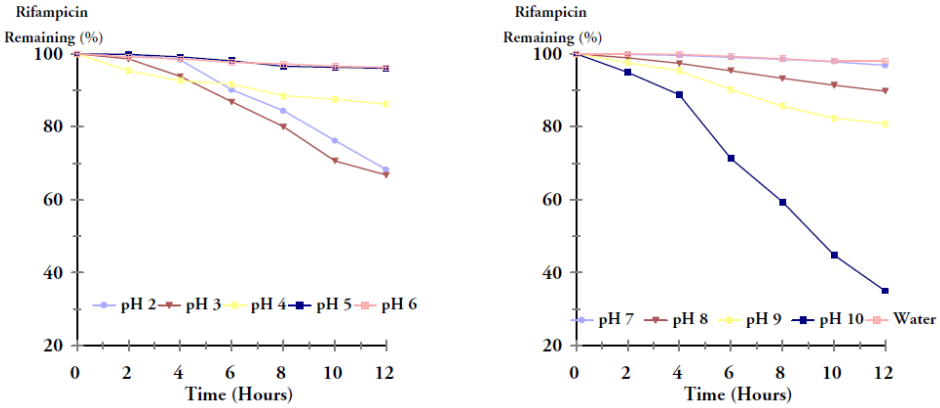

pH stability profiles of Rifampicin

d) Dissolution study

Rifampicin was dissolved in 20 ml of water and shaken continuously for 72 hours at 25 EC in a "shaker water bath". HPLC analysis was used to gather the experimental data during a 72-hour period. The medications were discovered to dissolve to their maximal concentration without starting a significant degree of degradation after 12 hours. Therefore, the 12-hour saturation approach will be used in the remaining solubility investigations.

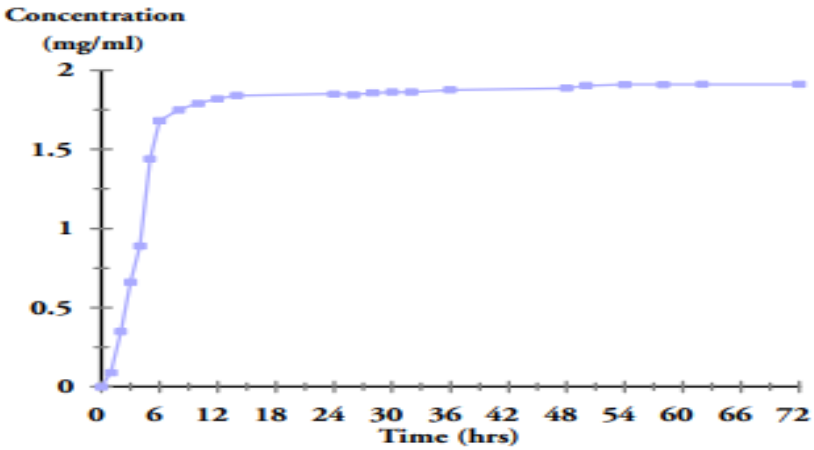

Dissolution: Rifampicin solubility time curve

- **Partition Coefficient (logP)**

At 0.1M electrolyte concentration, the partition coefficient (logP) was estimated using the consensus approach. According to the logP value rifampicin is lipophilic,

Partition coefficient of Rifampicin

Drug	logP
Rifampicin	2.78

Physical and chemical analysis of drug-loaded nanoparticles

Particle size, distribution and zeta potential

The synthesized PLGA NPs and SLN's particle size, polydispersity index (PI), and ZP values are shown in Tables below. Controlling particle size, PZ, and PI, permitting optimizing drug release and drug encapsulation, to obtain a site-specific regimen at a specified dosage, are the main objectives in the formulation of polymeric and solid-lipid nanoparticles. The "emulsion-solvent evaporation method" served as the foundation for the NPs production. For medications that are insoluble in water, this approach is often utilized.

Physicochemical characterization of drug loaded SLN

Characterization	Rifampicin
Partical size	180-300nm
Drug encapsulation efficiency (%)	56.997±2.72
Polydispersity index	0.328±0.04
Drug loading (mg/g polymer)	570±22
In vitro release (% of encapsulated drug)	Burst release 40-45 (%)
Zeta potential	−34.12 ± 1.06

Particle size, drug encapsulation effectiveness, zeta potential, drug loading capacity, polydispersity index, and invitro release of an encapsulated drug are a few examples of the physiochemical characteristics that were stated.

PLG NPS Drug loaded nanoparticles

Physicochemical characterization of drug loaded PLG-NP

Characterization	Rifampicin
Particle size	<200nm
Drug encapsulation efficiency (%)	45.22 ± 2.14
Polydispersity index	0.322 ± 0.004
Drug loading (mg/g polymer)	532±24
In vitro release (% of encapsulated drug)	3-8% burst release
Zeta potential	−30.06 ± 2.45

The solid-lipid nanoparticle-loaded PLG-NPs for rifampicin was shown in table below along with its physicochemical characterization. Drug loading capacity, particle size,drug encapsulation effectiveness, zeta potential, polydispersity index, and invitro liberation of an encapsulated drug are a few examples of the physiochemical characteristics that were stated.

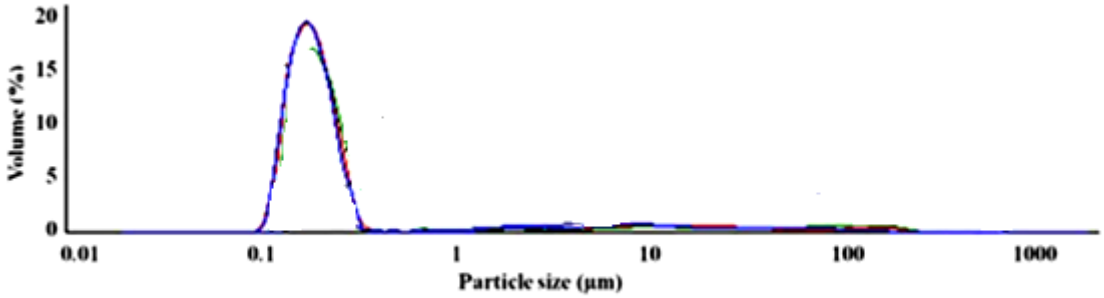

Particle size distribution of drug loaded PLGA NPs after formulation

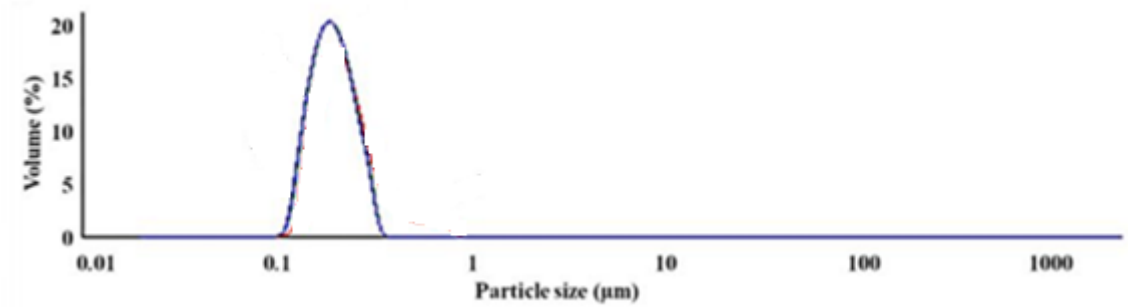

Particle size distribution of drug loaded SLN after formulation

Zeta potential

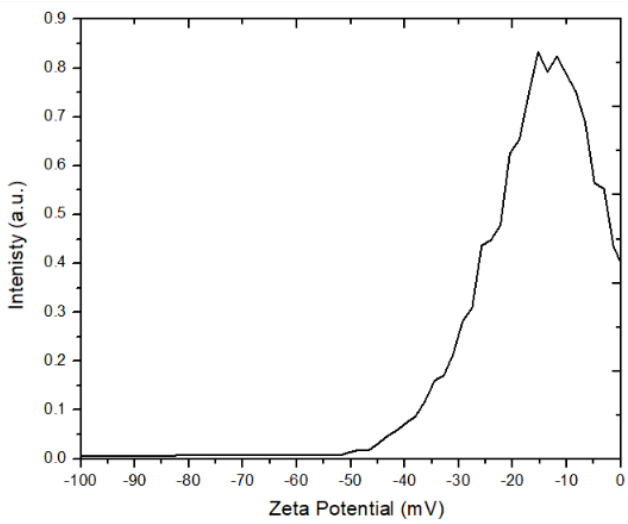

Zeta potential of PLGA nanoparticles loaded with Rifampicin

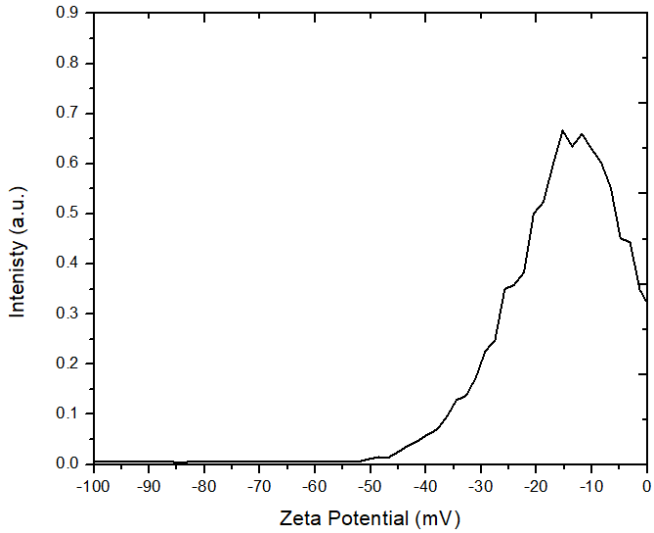

Zeta Potential of SLN nanoparticles loaded with Rifampicin

MORPHOLOGICAL ANALYSIS

X-RAY Diffraction (Xrd)

Individual drug-loaded PLA NPs showed strong peaks in their XRD patterns at 2 scattering angles of 15.695, 15.336, 19.615, 27.221, and 28.323, showing that they were crystalline in nature. The appearance of peaks at 2 distributed angles of 21.5 (insignificant) shows, however, that an amorphous halo was generated un all the SLNs, although with a diminishing degree of amorphicity. On the other hand, the peak was seen 17.523, 16.124, 18.542, and 23.321 un SLN.

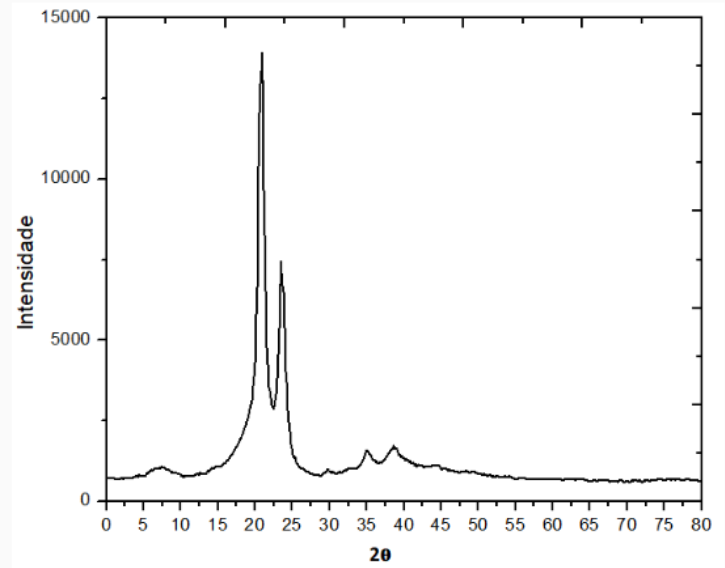

XRD patterns individual of drug loaded SLN SLN- rifampicin

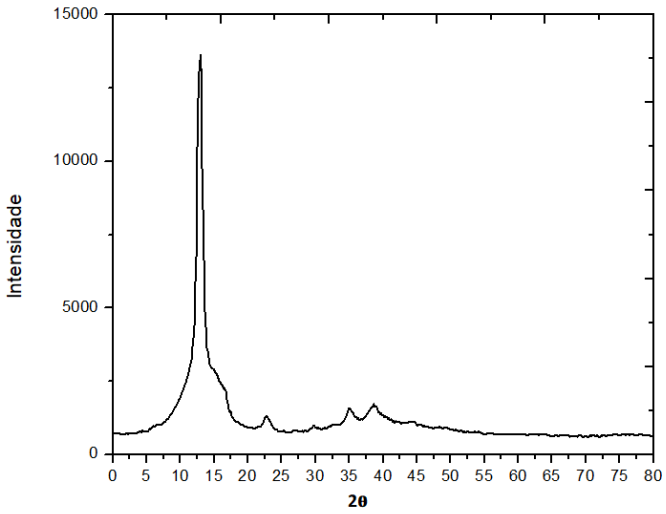

XRD patterns of PLGA NPs rifampicin

TEM (Transmission electron microscope) analysis

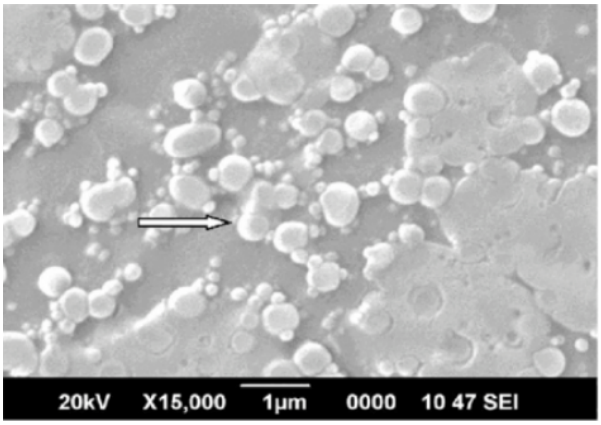

TEM analysis of drug loaded SLNPs Rifampicin

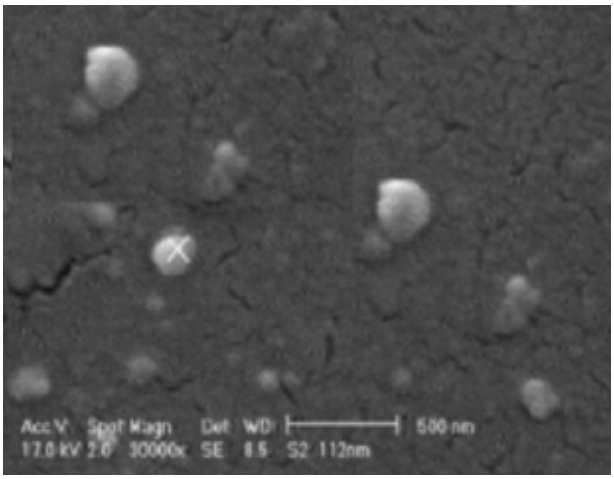

TEM analysis of drug loaded PLGA NPs Rifampicin

IN-VITRO DRUG RELEASE STUDIES

In-vitro release rate (SLN NPs)

Rifampicin: Similar to pyrazinamide, no rifampicin has released at 0 minutes. The release rate increases steadily, with 26.4% released at 60 minutes, 50.1% at 180 minutes, and 72.3 % at 360 minutes.

Drug loaded nanoparticles	% Drug Releases					
	0 min	30 min	60 min	120min	180 min	360 min
Rifampcin	0	18.2	26.4	41.7	50.1	72.3

In-vitro release studies- (PLGA NP's)

Rifampicin: Similar to pyrazinamide, the releases of rifampicin start with 0% at 0 minutes. The release rate increases progressively with time. At 30 minutes, 16.7% of drug has released, which further increases to 48.7% at 180 minutes and 62.2% at 360 minutes.

Drugloaded nanoparticles	% Release Rate					
	0 min	30 min	60 min	120 min	180 min	360 min
Rifampcin	0	16.7	21.2	33.4	48.7	62.2

Conclusion

The study entails creating and analysing nanoparticles that are loaded with a substance that has anti-tubercular action. There are two different kinds of nano particles: PLGA nanoparticles and solid-lipid nanoparticles. The effectiveness of these drug- loaded nanoparticles towards TB was examined in In vitro tests. The research may have an impact on how drugs are delivered and how TB patients are treated.

References

1. Parry CM. Epidemiological and clinical aspects of human typhoid fever. Salmonella infections: Clinical, immunological and molecular aspects. 2006 Nov 15:1-8.
2. A. Santos-Longhurst, "Types of Tuberculosis," Healthline.com, 2019. [Online]. Available: https://www.healthline.com/health/types-of-tuberculosis. [Accessed: Mar. 25, 2021].
3. Honish RL. Chest and Lung Diseases. InOver 55 2021 Dec 24 (pp. 81-100). Psychology Press.
4. Ganchua SK, White AG, Klein EC, Flynn JL. Lymph nodes—The neglected battlefield in tuberculosis. Advances in Surgical and Medical Specialties. 2023 Jul 14:143-66.
5. López-López JP, Posada-Martínez EL, Saldarriaga C, Wyss F, Ponte-Negretti CI, Alexander B, Miranda-Arboleda AF, Martínez-Sellés M, Baranchuk A, Neglected Tropical Diseases, Other Infectious Diseases Affecting the Heart (the NET-Heart Project). Tuberculosis and the heart. Journal of the American Heart Association. 2021 Apr 6;10(7):e019435.
6. H. W. Griffith, Complete Guide to Symptoms, Illness and Surgery. New York, NY, USA: Penguin, 2006.
7. Siggins MK, Sriskandan S. Bacterial lymphatic metastasis in infection and immunity. Cells. 2022 Jan;11(1):33.
8. Morimoto Y, Routes JM. Granulomatous disease in common variable

immunodeficiency. Current allergy and asthma reports. 2005 Sep;5(5):370-5.
9. Campbell JR, Winters N, Menzies D. Absolute risk of tuberculosis among untreated populations with a positive tuberculin skin test or interferon-gamma release assay result: systematic review and meta-analysis. bmj. 2020 Mar 10;368.
10. C. R. Horsburgh Jr., “Priorities for the treatment of latent tuberculosis infection in the United States,” N. Engl. J. Med., vol. 350, pp. 2060–2067, 2004.
11. American Thoracic Society, "Targeted tuberculin testing and treatment of latent tuberculosis infection," Am. J. Respir. Crit. Care Med., vol. 161, pp. S221–S247, 2000.
12. A. Koul, E. Arnoult, N. Lounis, et al., "The challenge of new drug discovery for tuberculosis," Nature, vol. 469, pp. 483-490, 2011. https://doi.org/10.1038/nature09657
13. G. A. Marriner et al., The medicinal chemistry of tuberculosis chemotherapy, Third World Diseases, pp. 47-124, 2011.
14. Duarte Y, Márquez-Miranda V, Miossec MJ, González-Nilo F. Integration of target discovery, drug discovery and drug delivery: a review on computational strategies. Wiley Interdisciplinary Reviews: Nanomedicine and Nanobiotechnology. 2019 Jul;11(4):e1554.
15. Dudek AZ, Arodz T, Gálvez J. Computational methods in developing quantitative structure-activity relationships (QSAR): a review. Combinatorial chemistry & high throughput screening. 2006 Mar 1;9(3):213-28.